Supplement of Aerosol Research, 3, 521–534, 2025 https://doi.org/10.5194/ar-3-521-2025-supplement © Author(s) 2025. CC BY 4.0 License.





Supplement of

$Condensation \ diffusion \ charging-particle \ number \ measurement \ of \ high \ concentrations \ down \ to \ 3 \ nm$

Helmut Krasa et al.

Correspondence to: Alexander Bergmann (alexander.bergmann@tugraz.at)

The copyright of individual parts of the supplement might differ from the article licence.

Particle growth analysis

While the Kelvin equation assumes nucleation in a uniform medium, free from the influence of external surfaces, heterogeneous nucleation involves the presence of pre-existing surfaces, such as nucleation seeds, which fundamentally alter the nucleation process.

Here, the presence of nucleation seeds reduces the energy required to form a cluster compared to homogeneous nucleation. Assuming spherical geometry of the seed particle, the Gibbs free energy for heterogeneous nucleation can be expressed as the Gibbs free energy for homogeneous nucleation multiplied by a contact parameter:

$$\Delta G_{\text{het}} = \Delta G_{\text{hom}} f(m, z) \tag{S1}$$

This contact parameter is based on geometric considerations:

$$f(m,z) = \frac{1}{2} \left(1 + \left(\frac{1 - mz}{g} \right)^3 + z^3 \left[2 - 3 \left(\frac{z - m}{g} \right) + \left(\frac{z - m}{g} \right)^3 \right] + 3mz^2 \left(\frac{z - m}{g} - 1 \right) \right)$$
 (S2)

With
$$g=(1+z^2-2mz)^{\frac{1}{2}},\, m=\cos\theta$$
 and $z=\frac{d_s}{d_p}$

The particle activation depends on the contact angle θ , the diameter of the seed particle d_s and the diameter obtained using the Kelvin theory d_p . The contact angle θ , defined at the solid-liquid-vapor interface, is used to describe the wettability of the surface (Fletcher, 1958). This allows to include the affinity between the WF and the seed particle, which induces a change in the size-dependent activation probability compared to the Kelvin theory. A lower contact angle between the liquid and the particle material indicates increased wettability and therefore a more favourable nucleation environment (Mamakos et al., 2011).

To derive a CE based on heterogeneous nucleation theory, further considerations are required. Knowing the Gibbs free energy of heterogeneous nucleation allows to calculate the nucleation rate, at which critical embryos form and subsequently develop into macroscopic droplets:

$$J_{\text{het}} = K_{\text{het}} e^{-\frac{\Delta G_{\text{het}}}{k_B T}} \tag{S3}$$

Here, k_B is the Boltzmann constant, K represents the kinetic prefactor, which is approximated as $K_{\text{het}} = \pi d_p^2 \times 10^{25}$ (Fletcher, 1958).

The activation probability can then be calculated. This represents the probability of nucleation occurring after time t:

$$P_{d_p, \text{het}}(t) = 1 - e^{(-J_{\text{het}}t)}$$
 (S4)

Seed particles are assumed to be activated if the activation probability is 0.5 or greater (Lauri, 2006).

The subsequent growth of activated particles is governed by the balance of mass and heat transfer processes at the droplet interface.

Following particle activation, the droplet grows along its trajectory at the following rate:

$$\frac{d\,d_p}{dt} = \frac{4D\nu_m\chi}{RT} \cdot \frac{p - p_p}{d_p} \tag{S5}$$

D is the diffusion coefficient, and χ is the correction factor outside the continuum regime. p_p is the equilibrium vapor pressure at the droplet surface of the surrounding gas with the pressure p at the current particle position. With the Fuchs-Sutugin approach (Davis, 1982), the value of χ is given as:

$$\chi = \frac{1 + Kn}{1 + 1.71Kn + 1.333Kn^2} \tag{S6}$$

Kn is the Knudsen number $Kn=2\lambda/d_p$. λ is the mean free path of molecules in the air. The vapor pressure at the droplet surface is:

$$p_p = p_s(T_p) \exp\left(\frac{4\sigma v_m}{RT_p d_p}\right) \tag{S7}$$

 p_s is the saturation vapor pressure of the WF. T_p is the temperature at the droplet surface and changes due to condensation on the droplet surface and is therefore dependent on the condensation rate $d d_p/dt$:

$$\frac{dT_p}{dt} = \frac{3}{c_p \rho d_p} \left(H_{vap} \rho \frac{dd_p}{dt} - 4k_g \frac{(T_p - T)\chi_h}{d_p} \right) \tag{S8}$$

The material parameters of the WF are the heat capacity c_p , density ρ , the latent heat of vaporization H_{vap} and the thermal conductivity of the surrounding gas k_q . χ_h corrects for heat transfer outside of the continuum regime:

$$\chi_h = \left(1 + \frac{2k_g}{\alpha_t d_p \rho_g c_{pg}} \sqrt{\frac{2\pi m_g}{RT}}\right)^{-1} \tag{S9}$$

The first term describes the latent heat added due to condensation resulting from the phase change of the WF from gaseous to fluid. The second term describes the heat flux of the hotter droplet towards the surrounding gas. The subscript g indicates the material parameters of the surrounding gas. m_g , ρ_g and c_{pg} are the average molecular mass, density and heat capacity, respectively. The thermal accommodation coefficient α_t was assumed to be one according to Seinfeld and Pandis (2016) who give a more in-depth description of the particle growth rate.

Measurement of Induced Currents

Typically, Farady cup electrometers (FCEMs) use a filter to collect particles on a filter and measured the resulting current. Fierz et al. (2014) used an open FCEM for contactless measurement of the aerosol charge. The total charge state of the aerosol

within the FCEM changes periodically with the corona pulse. This change (dQ/dt) induces geometry-dependent space charges and therefore a measurable current between the open FCEM and ground, eliminating the need for particle collection on a filter. The differential nature of this method reduces sensitivity to thermal and long-term drift. However, as the induced current is differential, the signal amplitude is influenced by the pre-existing charge state of the aerosol, which is particularly significant for smaller particles (Knoll et al., 2021). Furthermore, the temporal resolution of the PN measurement is limited by the pulse duration of the corona, which should be exactly as long as the gas exchange time within the FCEM to maximize the signal amplitude.

Fierz et al. (2008) incorporated a diffusion stage precipitator between the charger and an electrometer. By measuring the current at two stages, they could estimate the average particle size and thereby determine the PN concentration. Schriefl et al. (2020) employed a different technique, using a, electrostatic precipitator to progressively remove larger particles to offset their greater charging efficiency. The mobility scales differently with size in different regimes, d^{-2} in the molecular regime and d^{-1} in the continuum regime. The precipitator thus reduces the influence of the particle size on the measured current. Applying an appropriate voltage allows the precipitator to partially remove particles based on their electrical mobility, where larger particles are precipitated at a higher rate. Across a limited range, the measured average charge per particle becomes almost independent of the particle size, allowing for measurement of the PN concentration.

The instrument described in this work uses a DC operating in the modulated precipitation mode. In this mode, the charger operates continuously, while the voltage on the precipitator is periodically switched ON and OFF. This approach was chosen over pulsing of the corona for its operational stability within our instrument configuration. Since the detector is operated in the mode where the induced current is measured, the stationary current is zero when the precipitator is continuously ON or OFF. The sensor signal is therefore proportional to the change in the induced current when the precipitator state is modulated:

$$\Delta I_{MP} = I^{PREC_{ON}} - I^{PREC_{OFF}} \tag{S10}$$

where ΔI_{MP} is the total change in electrical current, $I^{PREC_{ON}}$ is the current measured with the precipitator activated and $I^{PREC_{OFF}}$ is the current measured with the precipitator off.

Typically, the modulated precipitation mode is used with the goal of achieving a size-independent PN measurement. This is achieved by tuning the precipitation voltage to flatten the size response, as described above. However, the preceding condensation stage in the CDC fundamentally changes the requirements. The condenser stage grows incoming particles into relatively large, monodisperse droplets, up to several µm, before they enter the charger and FCEM.

Since the droplets are nearly monodisperse, the need to compensate for size dependency of the DC is eliminated. Instead, the goal is to maximize the measurement signal ΔI_{MP} . Maximum signal strength is achieved when all particles are fully precipitated upon activating the precipitator ($I^{PREC_{ON}}=0$). Full precipitation can be achieved by setting the precipitator voltage sufficiently high or reducing the flow rate to ensure adequate residence time for precipitation. A reduction in flow rate would increase the gas exchange time in the FCEM, and therefore also the response time of the instrument. Therefore, the precipitation voltage was increased to ensure total precipitation of all particles.

Particle Droplet Evaluation

Table S1. Table of measured droplet sizes after condensational growth.

Seed Diameter [nm]	10	20	30	50	80	100	120	Average
Geom. Mean Diameter [µm]	1.9	1.95	1.92	1.92	1.9	1.99	1.97	1.94
Geom. Std. Dev. [1]	1.14	1.09	1.08	1.17	1.12	1.12	1.12	1.12

Saturation profile and particle activation

Particle activation at four different temperature settings at a constant $\Delta T = 35$ °C show a minor influence of the saturator and condenser temperatures on the d_{50} value, which varied by less than 0.3 nm.

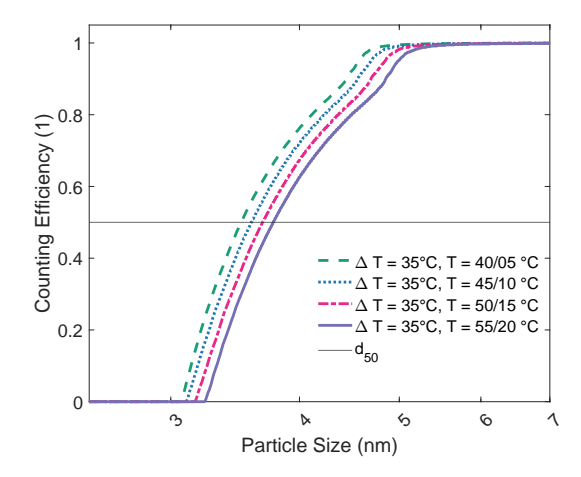


Figure S1. Simulated particle activation activation curves at a constant temperature difference between saturator and condenser (ΔT).

Simulated supersaturation, vapor concentration and particle activation data are shown.

The supersaturation profile shows a higher peak supersaturation for a larger ΔT , whereas the total vapor concentration and therefore particle growth rate, is mainly determined by the saturator temperature T_S .

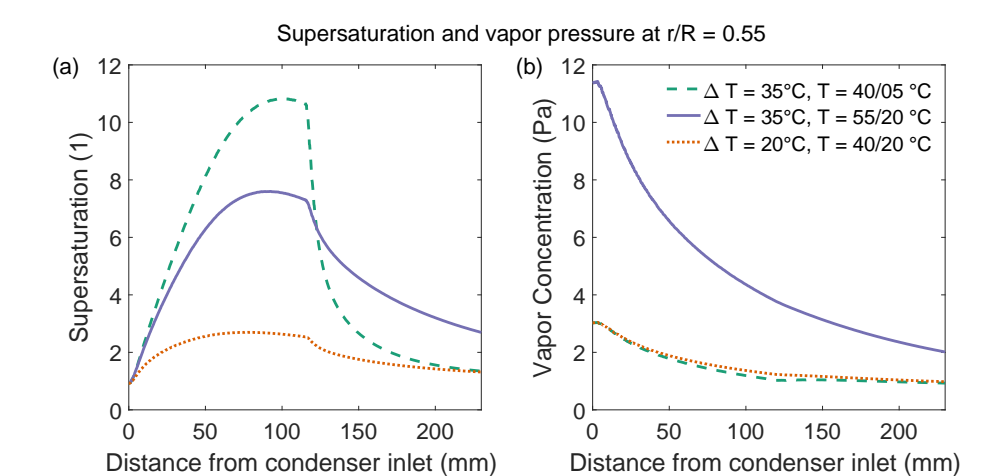


Figure S2. (a) Supersaturation and (b) vapor concentration profile along the growth axis for the three modeled temperature settings.

The simulated supersaturation profile and particle activation closely correlate and show, as expected, a maximum supersaturation at the center of the condenser. Particle sizes within the transition zone of the CPC (CE < 1) only activate up to a certain distance from the centerline of the condenser.

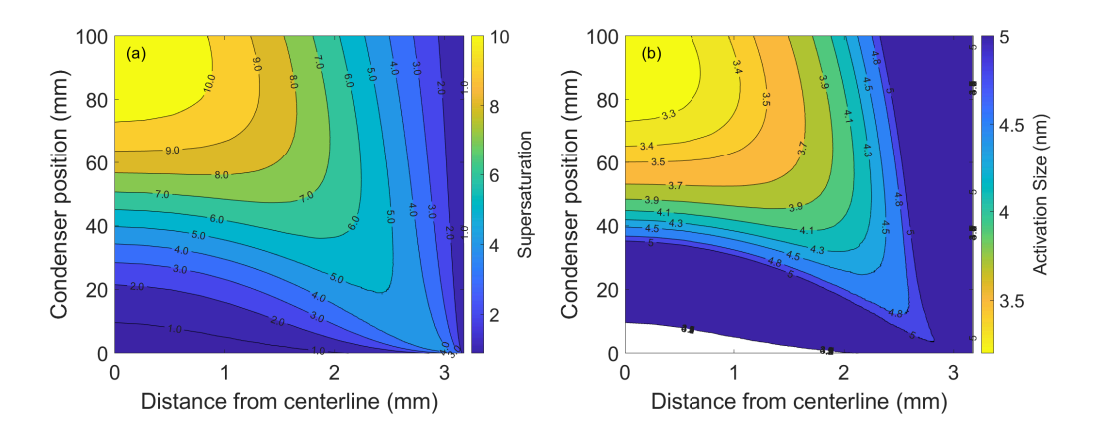


Figure S3. Contour plots of the (a) supersaturation field and (b) equilibrium Kelvin diameter of the condenser at a temperature setting of $T_s = 55$ °C and $T_c = 20$ °C

Furthermore, particle activation at a temperature setting of $T_c = 40$ °C and $T_S = 20$ °C was evaluated experimentally with DEG and shows good agreement with results obtained by the simulation. Particle counting was performed using a 23 nm CPC used as detection unit. The CPC was evaluated prior without the condensation stage prior and was found to have a d_0 value of 14 nm with Ag particles and was therefore suitable to evaluate the activation efficiency of the condensation stage without characterizing the CE of the charger.

The fitted d_{50} activation diameter was determined to be 9.5 nm. This value lies between the theoretical predictions from heterogeneous nucleation theory: 7 nm for perfect wetting conditions ($\theta = 0^{\circ}$) and 10.2 nm for a contact angle of $\theta = 20^{\circ}$.

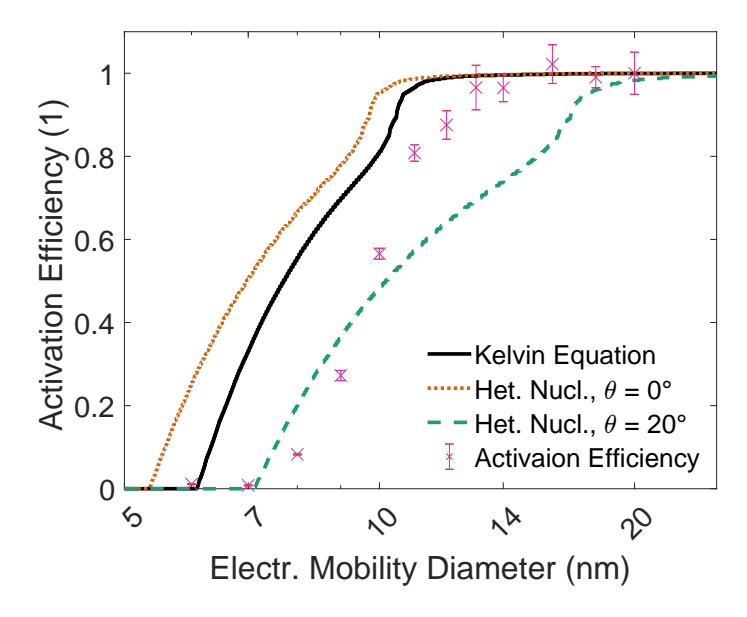


Figure S4. Activated particle sizes of the condensation stage at a temperature setting of $T_c = 40$ °C and $T_s = 20$ °C with Ag aerosol.

Concentration-dependent response for glycerol

Due to the lower temperature settings and reduced vapor pressure of glycerol, the droplet size was significantly smaller and the amplification was a factor of 4 compared to 20 with DEG at the default saturator temperature of T = 55 °C. Furthermore, due to reduced influence of concentration-dependent effects, the droplet size is not reduced for concentrations up to $> 10^5$ cm⁻³.

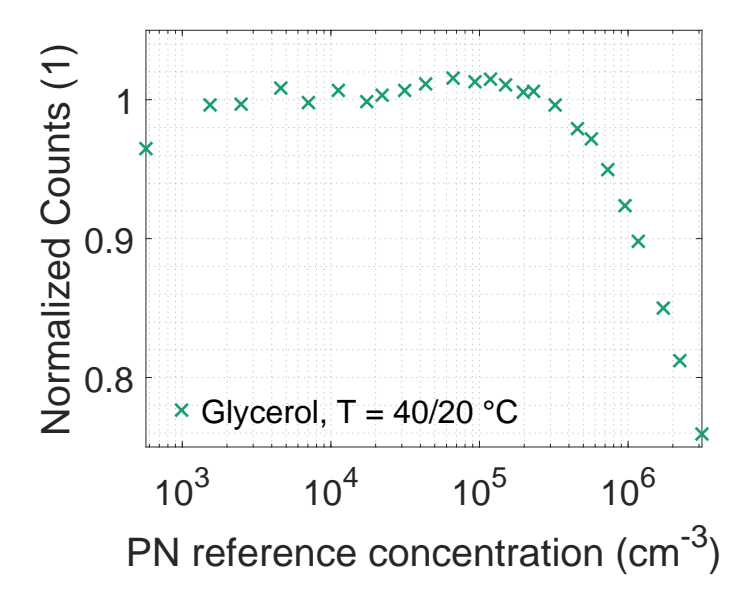


Figure S5. Linear response with glycerol as working fluid at a saturator and condenser temperature of T=40 °C and T=20 °C.

Chassis dynamometer measurements

To enable a direct comparison between the two instruments, the CDC was positioned parallel to the CPC, downstream of the sampling system. In this configuration, both devices measured the solid PN concentration. As the sampled carrier gas is identical (assuming adequate mixing before the flow is split up), a slight improvement in the tracking of the cumulative PN concentration and a better correlation of the detected emission peaks was achieved. The increased peak correlation yielded an \mathbb{R}^2 value of 0.94. Given the low concentration range measured by the CDC, the concentration-dependent fit function obtained from the measurement points in Figure 6 was not required.

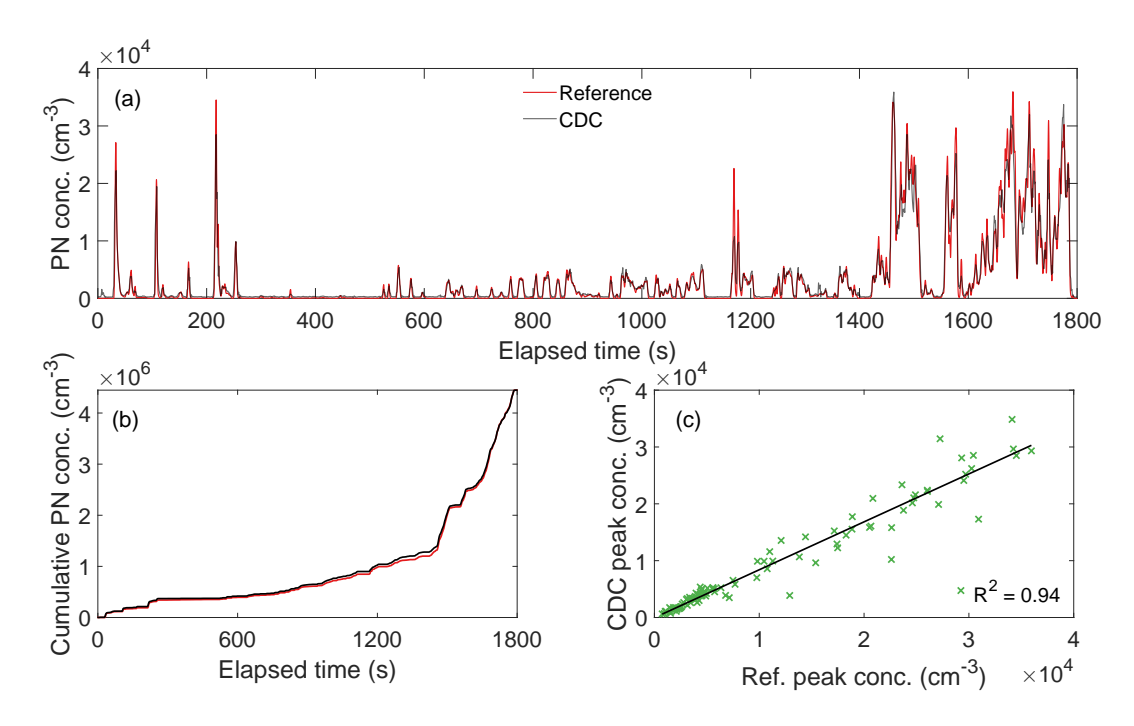


Figure S6. Calibrated results from the chassis dynamometer test. (a) Time-dependent measured concentration in the CVS tunnel of both the CDC counter and a reference counter. (b) Background-adjusted the cumulative PN concentration of both counters. (c) Correlation of detected emission peaks.

References

- Davis, E. J.: Transport phenomena with single aerosol particles, Aerosol Science and Technology, 2, 121–144, https://doi.org/10.1080/02786828308958618, 1982.
- Fierz, M., Burtscher, H., Steigmeier, P., and Kasper, M.: Field Measurement of Particle Size and Number Concentration with the Diffusion Size Classifier (Disc), SAE Technical Papers, https://doi.org/10.4271/2008-01-1179, 2008.
- Fierz, M., Meier, D., Steigmeier, P., and Burtscher, H.: Aerosol measurement by induced currents, Aerosol Science and Technology, 48, 350–357, https://doi.org/10.1080/02786826.2013.875981, 2014.
- Fletcher, N. H.: Size Effect in Heterogeneous Nucleation, The Journal of Chemical Physics, 29, 572–576, https://doi.org/10.1063/1.1744540, 1958.
- Knoll, M., Schriefl, M. A., Nishida, R. T., and Bergmann, A.: Impact of pre-charged particles on steady state and pulsed modes of unipolar diffusion chargers, Aerosol Science and Technology, 55, 512–525, https://doi.org/10.1080/02786826.2021.1873910, 2021.
- Lauri, A.: Theoretical and Computational Approaches on Heterogeneous Nucleation, Ph.D. thesis, University of Helsinki, ISBN 9525027775, ISSN 0784-3496, http://ethesis.helsinki.fi, 2006.
- Mamakos, A., Giechaskiel, B., Drossinos, Y., Lesueur, D., Martini, G., Krasenbrink, A., and European Commission. Joint Research Centre. Institute for Energy and Transport.: Calibration and modeling of PMP compliant condensation particle counters., European Comission, ISBN 9789279226106, https://doi.org/10.2788/41597, 2011.
- Schriefl, M. A., Nishida, R. T., Knoll, M., Boies, A., and Bergmann, A.: Characterization of particle number counters based on pulsed-mode diffusion charging, Aerosol Science and Technology, 54, 772–789, https://doi.org/10.1080/02786826.2020.1724257, 2020.
- Seinfeld, J. H. and Pandis, S. N.: Atmospheric Chemistry and Physics: From Air Pollution to Climate Change, Wiley-VCH, New York, 3rd edn., ISBN 978-1-118-94740-1, 2016.